October 29, 2013 | vol. 110 | no. 44 | pp. 17756–17761

PNAS

Proceedings of the National Academy of Sciences of the United States of America www.pnas.org

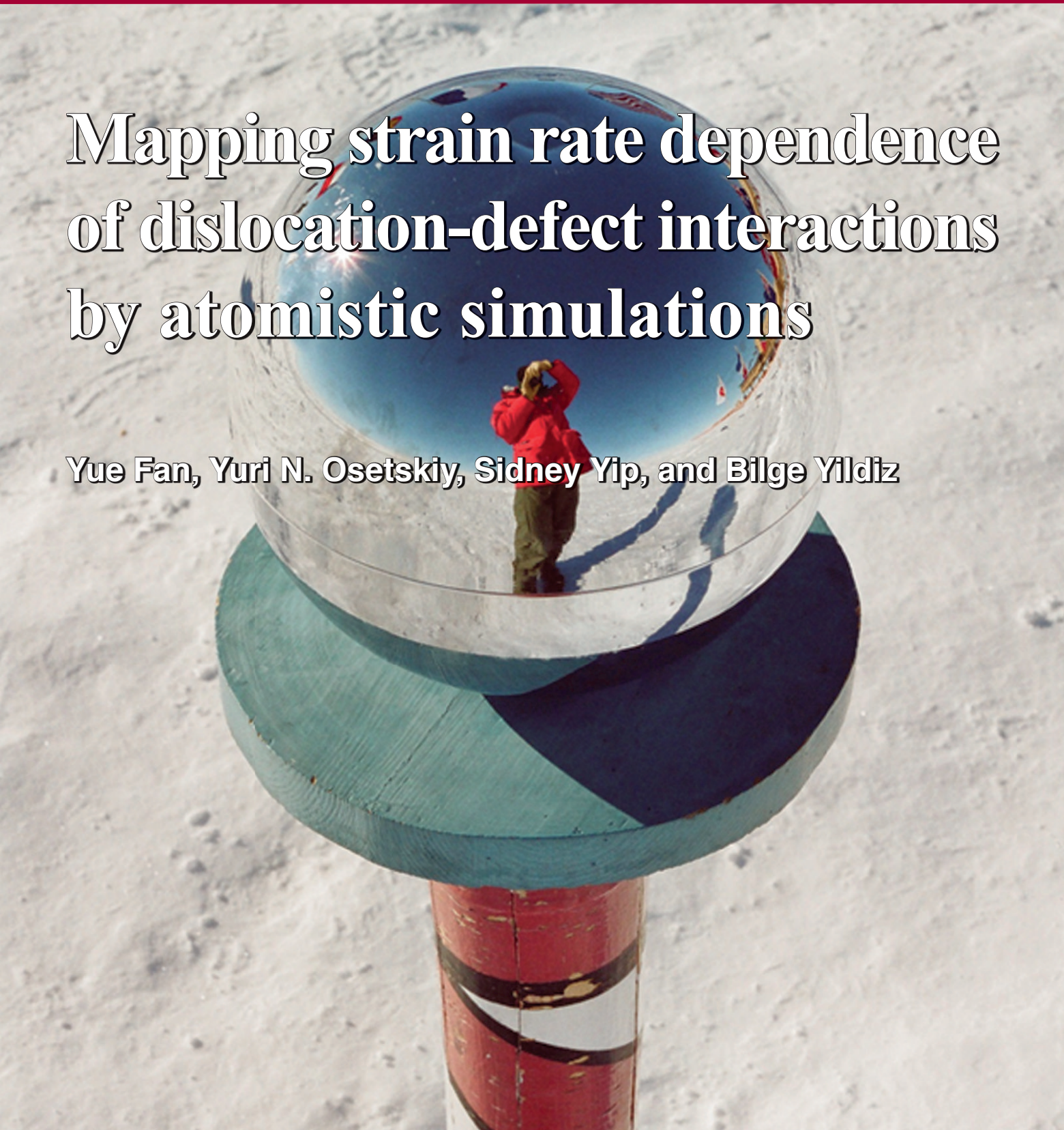

Mapping strain rate dependence of dislocation-defect interactions by atomistic simulations

Yue Fan, Yuri N. Osetskiy, Sidney Yip, and Bilge Yildiz

Mapping strain rate dependence of dislocation-defect interactions by atomistic simulations

Yue Fan[a], Yuri N. Osetskiy[b], Sidney Yip[a,c], and Bilge Yildiz[a,1]

[a]Department of Nuclear Science and Engineering and [c]Department of Materials Science and Engineering, Massachusetts Institute of Technology, Cambridge, MA 02139; and [b]Materials Science and Technology Division, Oak Ridge National Laboratory, Oak Ridge, TN 37831

Edited* by John P. Hirth, professor emeritus, Washington State University, Pullman, WA, and approved September 9, 2013 (received for review May 27, 2013)

Probing the mechanisms of defect–defect interactions at strain rates lower than 10^6 s^{-1} is an unresolved challenge to date to molecular dynamics (MD) techniques. Here we propose an original atomistic approach based on transition state theory and the concept of a strain-dependent effective activation barrier that is capable of simulating the kinetics of dislocation–defect interactions at virtually any strain rate, exemplified within 10^{-7} to 10^7 s^{-1}. We apply this approach to the problem of an edge dislocation colliding with a cluster of self-interstitial atoms (SIAs) under shear deformation. Using an activation–relaxation algorithm [Kushima A, et al. (2009) *J Chem Phys* 130:224504], we uncover a unique strain-rate–dependent trigger mechanism that allows the SIA cluster to be absorbed during the process, leading to dislocation climb. Guided by this finding, we determine the activation barrier of the trigger mechanism as a function of shear strain, and use that in a coarse-graining rate equation formulation for constructing a mechanism map in the phase space of strain rate and temperature. Our predictions of a crossover from a defect recovery at the low strain-rate regime to defect absorption behavior in the high strain-rate regime are validated against our own independent, direct MD simulations at 10^5 to 10^7 s^{-1}. Implications of the present approach for probing molecular-level mechanisms in strain-rate regimes previously considered inaccessible to atomistic simulations are discussed.

structural materials | mechanical properties | low strain rate atomistic simulation

Interactions of defects with dislocations affect many mechanical properties of metals. This is especially important for irradiated materials where a host of nonequilibrium defect structures are produced. They act as obstacles to moving dislocations, alter the mechanical properties, and critically impact the safety and integrity of structural materials in nuclear energy systems (1–3). Molecular dynamics (MD) methods have proven to be useful in revealing the deformation mechanism with atomic-scale details (4), yet they are limited to a high strain-rate regime, about 10^6 s^{-1} and above. It is known that material deformation mechanisms are strongly affected by the applied stress, temperature, and grain size (5–7). Strain rate, another key factor, has been relatively less studied because of a significant time-scale gap between typical experiments and conventional atomistic simulations. Many tensile experiments are performed under low strain rates—that is, slower than 10^0 s^{-1} (8–10)—whereas MD simulations are limited to much higher strain rates, greater than 10^6 s^{-1} (4, 11–13), or to static conditions (1, 14, 15). In static calculations the system is relaxed by potential energy minimization, so thermal activation processes are excluded. In MD simulations thermal activation also can be suppressed because of the high strain rate. Thus, a correspondence may be expected between molecular statics and MD simulations at low temperatures (16–18). However, the equivalence can break down when the strain rates are so high in MD simulations that the system is driven out of equilibrium. For strain rate less than 10^8 s^{-1} and at low temperatures, an equivalence may hold between MD and static simulations (*SI Appendix*).

Generally, the high strain-rate results from MD are either directly compared with experiments (13) or incorporated into continuum approaches (19). An issue currently exists in reconciling the results of atomistic MD simulations with experiments because of the time-scale gap between them, whereas it is known that both strain rate and temperature affect the interaction mechanism and critical stresses (1, 4, 8, 12, 20–27). Methods alternative to MD exist, some based on surveying the potential energy surface coupled with variants of kinetic Monte Carlo (28, 29) and some based on escaping from the deep energy minima in dynamics simulations (30–32). To date these methods have not been used to study dislocation–obstacle interactions to any significant extent, except possibly for the case of an adapted activation–relaxation method known as Autonomous Basin Climbing (ABC) algorithm (18, 33).

An example to this issue is studied here in hcp Zr. Molecular static calculations, akin to simulations at high strain rate and low temperature (16–18), showed that an edge dislocation passes through a cluster of self-interstitial atoms (SIAs) under shear deformation, with both defects recovering their original structures after the interaction (1). On the other hand, in postmortem transmission electron microscopy (TEM) on irradiated Zr specimens deformed at low strain rates ($10^{-4}s^{-1}$) and high temperature (600 K), a formation of so-called cleared channels was observed. The entire plastic deformation was found to localize in these channels, which were completely free from defects (8). The presence of dislocation channels indicates the removal of the obstacles on the slip plane by the moving dislocations. Clearly there is a seeming discrepancy between the experiments and simulations.

Significance

Strain rate affects the dislocation interactions and plasticity in materials. Quantitative prediction of dislocation–defect interaction mechanisms and critical stresses as a function of strain rate, reaching down to the experimental deformation conditions much lower than 10^6 s^{-1}, has been an outstanding challenge to traditional atomistic simulations. This study provides an original analytical and atomistic approach to predict dislocation-defect microstructure evolution at arbitrarily low strain rates. We demonstrated this model on a specific defect–dislocation system in zirconium, where the results bridge simulations to experiments, a paradigm that has been prohibitive to molecular dynamics. The principles in this study are broadly applicable to assessing the effects of strain rate on other defects with increasing complexities in a range of materials.

Author contributions: B.Y. designed research; Y.F., Y.N.O., S.Y., and B.Y. performed research; Y.F. performed the new combination of ABC and TST calculations; Y.N.O. performed the MD simulations; Y.F., Y.N.O. and B.Y. analyzed data; and Y.F., S.Y. and B.Y. wrote the paper.

The authors declare no conflict of interest.

*This Direct Submission article had a prearranged editor.

[1]To whom correspondence should be addressed. E-mail: byildiz@mit.edu.

This article contains supporting information online at www.pnas.org/lookup/suppl/doi:10.1073/pnas.1310036110/-/DCSupplemental.

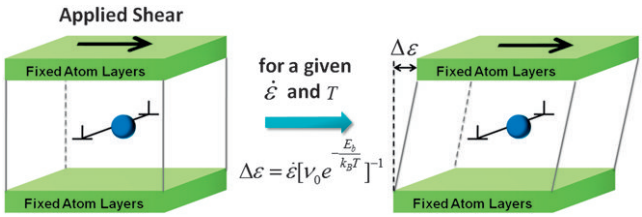

Fig. 1. Schematic of the simulation of dislocation–obstacle interaction under shear deformation at applied strain rate, $\dot{\varepsilon}$, and temperature, T. ν_0 is the attempt frequency, E_b is the predetermined effective activation barrier at each strain increment, and $\Delta\varepsilon$ is the calculated shear strain increment that is applied at each step of the simulation algorithm.

Recently, we have used the transition state theory (TST) approach to formulate the coupling of strain-rate effects to thermal activation in describing the mobility of an edge dislocation in a metal (18). Here we extend our formulation to predicting the mechanisms and kinetics of dislocation–defect interactions from atomistic simulations over a wide range of time scales including low strain rates. Our starting point is the sampling of interaction pathways and energies at the atomistic level using the ABC method (34–38). Combining the atomistic interaction pathways and energy barriers with TST, in what we now call ABC-T, enables us to span a wide range of time scales. We theoretically derive the impact of applied strain rate on the thermally activated interaction processes using TST, and inform the TST model by results from the ABC calculations. In this original approach (Fig. 1 and *Methods*), the simulation of dislocation–defect interactions can reach arbitrarily low strain rates, unlike the previous MD simulations that were limited to the very high strain-rate regime. This approach, when implemented in hcp Zr, enabled us to uncover dislocation–defect interaction mechanisms over strain rates from 10^{-7} s^{-1} to 10^{7} s^{-1}, well beyond the reach of traditional MD methods. We demonstrate the interplay between thermal activation and strain rate through an interaction mechanism map for hcp Zr. The results at high strain rates are then validated against MD simulations on the same defect system, and various mechanisms in other material systems can also be reasonably explained, as discussed later.

The article is laid out as follows. The basic modeling and simulation methodology is summarized in *Simulation Methodology*, with further details given in *Methods*. The unique feature introduced is the use of TST to determine the incremental strain step in evolving the system under a prescribed strain rate and temperature. To execute the simulation one needs to know the effective activation barrier at each step, calculated by ABC. Static simulation results of the dislocation–SIA cluster model under study are discussed in *Results of Static Simulation*, showing a recovery mechanism at high strain rates for the interaction similar to previous simulations. Results on dislocation–defect interactions at finite temperature and several strain rates are presented in *Simulation at Finite Temperature and Constant Strain Rates*. At the two lowest strain rates studied, a climb mechanism (defect absorption) associated with a trigger reaction appears, and this is different from the one seen at the higher strain rate (and in static simulations). In *Mechanism Map in Strain Rate and Temperature*, guided by our unexpected findings from the previous section, we determine separately the corresponding activation barrier and use this as input to a coarse-graining formulation to predict a mechanism map in strain rate and temperature. We show the predicted crossover from recovery to climb agrees quite well with our independent MD simulations in the high strain-rate regime. There are several implications regarding the significance of a mechanism map involving the strain rate as a state variable; they are discussed in *Discussion and Conclusion*.

Simulation Methodology

In this work we choose to study the interaction between a $1/3<11\bar{2}0>\{1\bar{1}00\}$ edge dislocation in the prism plane and a 5-SIA cluster in the basal plane of hcp Zr as a model system. We take an SIA cluster with a planar structure in the basal plane as an energetically favorable defect in Zr (39). For the dislocation, we take the prismatic slip system, found in tensile experiments to be more affected by irradiation than the basal slip system (8). In tensile test experiments, the system is strained by applying a controlled external strain rate. To mimic the experimental conditions, we apply the procedure illustrated in Fig. 1 and described in *Methods* to simulate the dislocation–defect interactions. The algorithm defined in *Methods* permits us to identify the dislocation–obstacle interaction mechanism and the critical shear stresses under different strain rates and temperatures, and to extend to arbitrarily lower strain rates than those possible with traditional MD. In summary, the present approach combines the TST framework with the activation–relaxation algorithm known as ABC for sampling interaction pathways and energies (34–38). The simulation proceeds in time step increments. Each incremental strain step is calculated by TST at a prescribed strain rate and temperature, given the reaction pathway and energy barriers (E_b) found by ABC calculations. The simulation is terminated when the dislocation is unpinned and the defect system is fully relaxed.

Results of Static Simulation

We first consider the dislocation–SIA interaction under static conditions. The results will provide a useful reference for the simulations at finite temperature and varying strain rates to follow. Fig. 2 shows the system-level response of defect interaction to shear deformation, variation of the shear stress with applied strain, and the corresponding atomic configurations. One can see two stress relaxation events over the course of strain deformation. The atomic configurations at points 2 and 3 indicate the first stress drop is associated with dislocation pinning to the SIA cluster. This pinning consists of a glide motion of the dislocation and a climb of the SIA cluster (Fig. 2*B*,

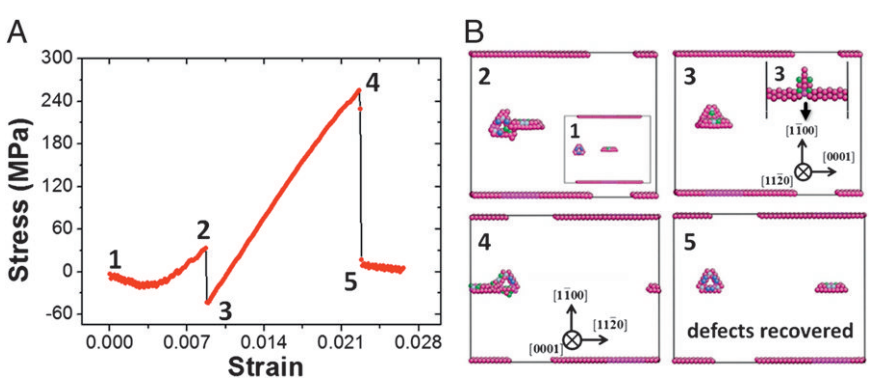

Fig. 2. (*A*) Stress–strain curve for the interaction between a $1/3<11\bar{2}0>\{1\bar{1}00\}$ prismatic edge dislocation and a basal 5-SIA cluster in hcp Zr. Atomic configurations at five indicated points are examined to reveal the interaction mechanism associated with each of the two sudden stress relaxation events. (*B*) The corresponding atomic configurations indicating dislocation–defect pinning and defect recovery at the first (2, 3) and second (4, 5) stress relaxations, respectively.

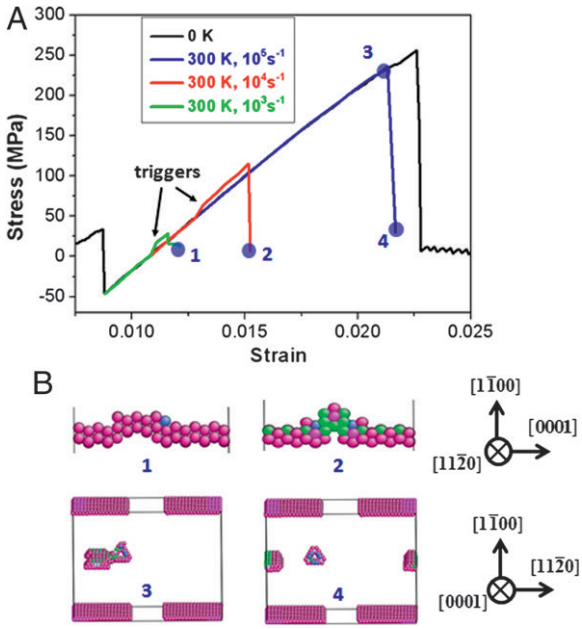

Fig. 3. (*A*) Stress–strain curves (in color) under different strain rate and temperature conditions, and (*B*) atomic configurations associated with points 1 through 4, as marked on the stress–strain curve.

configuration 3). Upon further straining, there is a monotonic increase of the stress from 3 to 4. The second stress reduction occurs at about 250 MPa, where the atomic configurations show clearly the dislocation and SIA cluster detach from each other. The dislocation structure is seen to be fully recovered after the interaction. Although the SIA cluster structure is also recovered, the interaction with dislocation has caused it to be shifted up by one plane above the original glide direction. Because the results of Fig. 2 are the same as those in a previous static simulation in a significantly larger system (1), they may be regarded as validation of our model setup and simulation procedure.

Simulation at Finite Temperature and Constant Strain Rates

We now study the same unit process of dislocation–SIA cluster interaction by applying the TST-based methodology described in *Simulation Methodology*. Simulations are conducted at 300 K, and three selected strain rates, 10^5 s^{-1}, 10^4 s^{-1}, and 10^3 s^{-1}. The attempt frequency is taken to be 10^{13} s^{-1}. Fig. 3*A* shows the effects of finite temperature and varying strain rates on the system-level response. Both temperature (thermal softening) and reducing strain rate contribute to lowering of the peak stress and the strain values associated with the onset of stress relaxation, which is physically what one would expect. On the stress–strain curve, it may appear that all three strain rates give the same qualitative behavior. However, this is not the case when one examines the corresponding atomic configurations at points 1, 2, and 4, at strain rates 10^3, 10^4, and 10^5 s^{-1}, respectively. As shown in Fig. 3, although the dislocation–SIA cluster interaction ended with the recovery of both defects for 10^5 s^{-1} (point 4), the interaction at the two lower strain rates result in absorption of the SIA cluster (points 1 and 2).

We will refer to the process occurring at the high strain rate of 10^5 s^{-1}, where the dislocation and SIA cluster structures reconstituted, as the "recovery" mechanism (albeit the cluster climbed to one plane higher). We will designate process at the lower strain rates, 10^4 s^{-1} and 10^3 s^{-1}, where the SIA cluster is absorbed, as the "climb" mechanism. In the latter, absorption by the dislocation is associated with a superjog formation, with the resultant jog being dragged along by the gliding dislocation. In the climb mechanism at 10^3 s^{-1}, the absorbed SIA cluster spreads into an extended jog structure (seen in configuration 1 in Fig. 3), whereas at the higher strain rate (i.e., 10^4 s^{-1}), the absorbed cluster takes on a narrow jog structure. The reason is that the SIA does not have enough time to spread out and fully interact with the dislocation at this relatively higher strain rate (seen in configuration 2 in Fig. 3).

It is important to know under what conditions the recovery and climb mechanisms dominate, as the latter can lead to creep and growth (2, 3), or to sweeping of defects and the formation of clear channels in the prism plane (40). To formulate a strain-rate criterion for the transition between these competing mechanisms, we examine further the results of Fig. 3. We focus on a reaction, to be denoted as the "trigger," that appears in the stress–strain curve at strain rates of 10^4 s^{-1} and 10^3 s^{-1} in connection with the climb mechanism. The trigger reaction is an activated and irreversible process involving the rearrangement of the local structure. The atomic configurations in the trigger reaction are shown in Fig. 4. One sees a few atoms on the bottom edge of the SIA cluster are pushed upwards, leaving behind a relatively low-density region near the dislocation core. The local free volume in turn facilitates rearrangement of the local atoms to assist the absorption of SIA cluster by the dislocation, as seen in Fig. 3 (configurations 1 and 2).

Whether the trigger reaction can take place or not is determined by the interplay between applied strain rate and temperature. To quantify this interplay we look for additional details concerning the thermally activated reaction paths and the corresponding energy barriers in the trigger reaction to understand how they are affected by the applied strain rate. As shown in Fig. 5, the trigger event can only occur with strain values from ε_i to ε_f (the light blue region in the figure). This is because before strain ε_i the dislocation and SIA cluster are not yet in contact with each other, whereas beyond ε_f the dislocation will just pass through the SIA cluster following the recovery mechanism. In the range $(\varepsilon_i,\varepsilon_f)$ the trigger barrier decreases initially with strain and reaches a minimum around 0.33 eV at the critical strain around 0.015. Beyond the minimum, the barrier increases with strain. The parabola-like shape seen in Fig. 5 can be traced to the symmetric distribution of the Burgers vector for the $1/3<11\bar{2}0>\{1\bar{1}00\}$ edge dislocation when using the Ackland–Wooding–Bacon (AWB95) potential (41) and the symmetric shape of the SIA cluster. This nonmonotonic behavior is distinctly different from the traditional picture of monotonic decrease of dislocation glide activation barrier (represented typically as $E_b(\varepsilon)=E_0[1-(\varepsilon/\varepsilon_c)^p]^q$, where E_0 is the barrier at zero strain/stress, ε_c is the yield strain, and p and q are shape parameters). The combination of a finite strain range (from ε_i to ε_f) for the trigger reaction and the existence of a nonzero minimum of the activation barrier essentially delineate a time window for the activated reaction to occur.

Mechanism Map in Strain Rate and Temperature

It is to be expected that the trigger reaction is an interplay between thermal and strain activations. If the strain rate is too high, there will not be enough time for thermal activation to be effective, so the trigger reaction cannot proceed. By the same token, a lower strain rate permits more time for the thermally activated trigger reaction to occur. Similarly, at higher temperature,

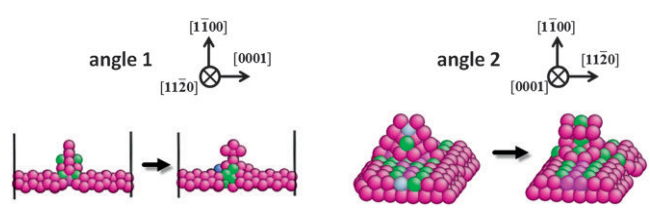

Fig. 4. The atomic structure involved in the appearance of the trigger reactions in the strain–stress curve in Fig. 3 for the condition of lower strain rates.

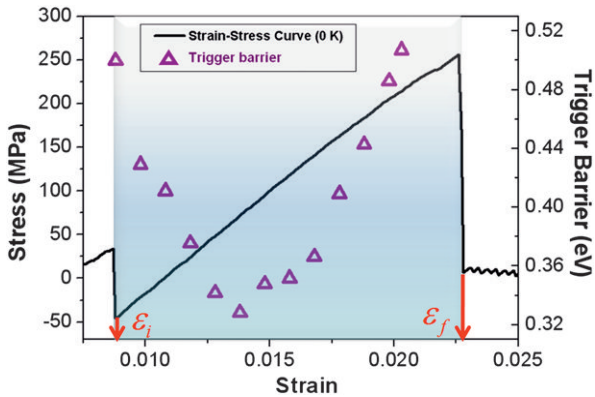

Fig. 5. The energy barrier for the trigger reaction that leads to dislocation jog via the absorption of the SIA cluster, shown here as a function of strain, superimposed on the strain–stress curve at 0 K from Fig.3. The trigger reaction can take place only between ε_i and ε_f.

less time is needed for activation, so the trigger reaction becomes more likely. We have previously discussed how thermal activation is affected by strain rate in the mobility of a screw dislocation in bcc Fe under shear (18). The key quantity in this study is the stress (or strain)-dependent activation energies, $E(\varepsilon)$, that allows temperature and rate effects to be coupled in the TST description of dislocation motion. In the same spirit and guided by the findings just described, we follow a procedure explained in detail in *Methods* to obtain the activation energy profile $E(\varepsilon)$, for the trigger reaction, shown in Fig. 5. An activation probability of the trigger event (see *SI Appendix* for the derivation) then can be calculated as a function of temperature and applied strain rate as:

$$P_{trigger}(T,\dot{\varepsilon}) = \frac{1}{\dot{\varepsilon}} \int_{\varepsilon_i}^{\varepsilon_f} k(\varepsilon) e^{-\frac{1}{\dot{\varepsilon}}\int_{\varepsilon_i}^{\varepsilon} k(\varepsilon')d\varepsilon'} d\varepsilon, \qquad [1]$$

where $k(\varepsilon) = \nu_0 e^{-E(\varepsilon)/k_B T}$ represents the thermal activation rate of the trigger event, $\dot{\varepsilon}$ is the applied strain rate, and ε_i and ε_f represent the initial and final strain states for the trigger interaction, respectively. We choose a threshold probability p_c for deciding whether the trigger reaction can be activated, with p_c being 0.5 or greater. If $P_{trigger} \geq p_c$, then the trigger event proceeds (climb mechanism dominant), whereas if $P_{trigger} < p_c$, the dislocation passes through the SIA cluster (recovery mechanism dominant).

The mechanism map so-constructed, shown in Fig. 6, delineates the two regions where recovery and climb mechanisms are expected to dominate. The boundary separating the two regions is obtained by evaluating Eq. **1** with $E(\varepsilon)$ given by the strain-dependent activation barrier shown in Fig. 5 and with $\nu_0 = 10^{13}\ s^{-1}$. The band surrounding the curve is obtained by allowing ν_0 to vary between $10^{12}\ s^{-1}$ and $10^{14}\ s^{-1}$. The results shown correspond to taking $p_c = \int_0^1 e^{-x}dx \approx 0.632$. A sensitivity analysis of the choice of p_c from 0.5 to 0.632 shows insignificant variation in the resulting mechanism boundary.

In Fig. 6 we also show the results of our MD simulations on the same dislocation–SIA cluster system at three strain rates (*Methods*). These simulations are computationally very demanding, especially the long runs required to reach a strain rate of $10^5\ s^{-1}$. The agreement between the independent MD simulations and the predicted mechanism map seen in Fig. 6 is quite remarkable. This consistency suggests that the basic arguments used in our analysis of coupled thermal and stress activation effects are quantitatively accurate at least in the limit of high strain rates. To our knowledge, such analytical and quantitative testing of the atomistic theory of defect interactions against MD simulations has not been reported heretofore. Besides the high strain-rate regime, our formulation also extends to the low strain-rate regime relevant to many experiments on defect interactions and mechanical deformations. Quantitative validation against appropriate experiments would be worthwhile in future work. In Fig. 6 we show one statistical TEM study of dislocation channeling where defect absorption mechanisms play an important role (8). Strain rate and temperature have been observed to affect the dislocation–obstacle interactions in several previous reports (i.e., see ref. 4 and the references therein). However, the TST-based analytical approach presented here is able to quantitatively predict a mechanism map over a wide range of strain rates that was inaccessible to MD simulations to reach before.

A clearer picture of strain rate effects on defect interactions as presented here can help to reconcile previous experimental results and molecular static simulations. In the case of interaction between an <a> edge dislocation and a SIA cluster (the same type of defects as those modeled here) in Zr (1), simulation has shown the outcome to be the recovery mechanism. On the other hand, tensile experiments (8) at 600 K and $10^{-4}\ s^{-1}$ showed clear channels, indicating the climb mechanism is expected to operate (Fig. 6). The absorption and drag of SIA clusters by the dislocation can clear the obstacles along the dislocation path, thus providing an explanation of defect-free channels observed in the experiments. This means one should not regard the previous static simulations to be in conflict with experiments; rather they pertain to different regimes on the mechanism map. Our results demonstrate the magnitude of applied strain rate can be an important factor in the formation of dislocation channels. It is worth recalling here that the absorption of obstacle by dislocation is not the only mechanism for dislocation channeling. For example, in Cu, in the interaction between edge dislocation and stacking fault tetrahedra (SFT) with certain geometry, high temperature (>300 K) and low, in MD scale, strain rate ($<10^7\ s^{-1}$) (4), sessile jog can be transformed into glissile structures that can be dragged away by moving dislocations.

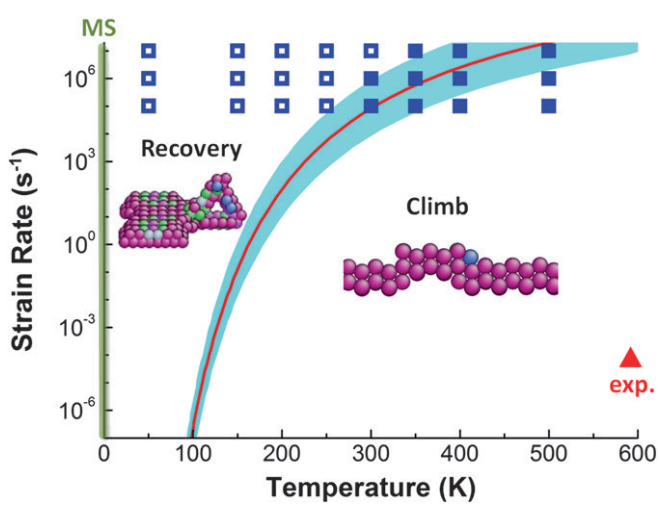

Fig. 6. (Mechanism map) The strain rate–temperature diagram showing the boundary separating the recovery and climb mechanisms in dislocation–SIA cluster interaction studied in this work in hcp Zr. Calculated boundary (red curve) is obtained using an attempt frequency of $10^{13}\ s^{-1}$. Upper and lower bound of the light blue region correspond to attempt frequencies of $10^{14}\ s^{-1}$ (upper bound) and $10^{12}\ s^{-1}$ (lower bound), respectively. The blue data points are the MD results, with the open squares representing the result of recovery mechanism and the filled squares representing the climb mechanism. The green line on the left denoted as "MS" represents the result from previous molecular static simulations (2), and the red triangle denoted as "exp." represents the result from experiments (9) as an outcome of dislocation–SIA cluster interactions in hcp Zr.

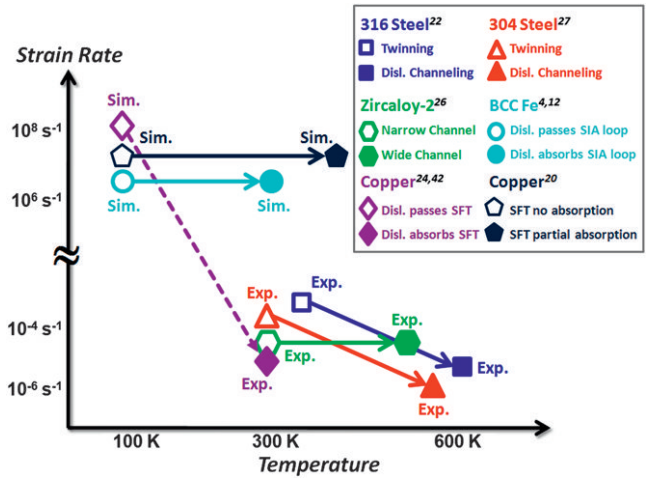

Fig. 7. A summary of selected experimental and computational data from different materials to show the transition from athermal deformations to thermally activated processes with reducing strain rate or with increasing temperature. The data on 316 stainless steel experiments are adapted from ref. 22, 304 stainless steel experiments from ref. 27, Zircaloy-2 experiments from ref. 26, copper experiments from ref. 24, copper simulations from refs. 20, 42, and bcc Fe simulations from refs. 4, 12.

Discussion and Conclusion

We have proposed a unique atomistic modeling framework that combines TST and ABC, ABC-T, to assess the dislocation–defect interaction mechanisms and critical stresses over a wide range of strain rate conditions. In so doing we extend time scales accessible to atomistic simulation beyond the range of traditional MD simulations by many orders of magnitude. We cast our results in a deformation mechanism map with strain rate as an independent control parameter. In studying dislocation–SIA cluster interaction in hcp Zr, we find two distinct competing interaction mechanisms as manifestations of the fundamental interplay between thermal activation and applied strain rate. Because the two mechanisms have different consequences on mechanical properties, we constructed a temperature–strain rate mechanism map, and the fundamental and quantitative understanding of such a mechanism map with regard to simulation versus experiment will have broad implications.

Our findings may be extended to other types of defects and classes of materials where atomistic simulation results are not yet entirely compatible with interpretations of experiments. Consider a similar situation in Cu, where a long-standing and inconclusive inquiry exists to understand the formation of clear channels upon interaction of dislocations with SFT. The SFTs were found to be collapsed by a single moving dislocation in in situ straining TEM experiments (23, 24), leading to the formation of defect-free regions. On the other hand, in early MD simulations, the dislocations were found to pass through the perfect SFTs without absorbing them (42). More recent MD simulations demonstrated the interaction is dependent on the geometry, temperature and strain rate, and boundary conditions (20, 25). It was shown that, in the presence of high temperature and free surfaces, the interaction can lead to a partial disappearance of SFT, which is qualitatively more consistent with the observations in the in situ straining TEM experiments. However, a complete disappearance of SFTs was never observed by MD but was often observed experimentally. It has been suggested the strain rate difference between experiments and MD simulations is the most probable reason for the discrepancies between these two sets of results (23). A mechanism map like Fig. 6 could provide a quantitative resolution of this apparent controversy. In Fig. 7 we show a collection of simulation and experimental results of dislocation–defect interactions for several metals. In each case there is a transition in mechanism (open to closed symbols) with either increasing temperature or decreasing strain rate. For example, in MD simulations of dislocation–SIA loop interaction in bcc Fe and of dislocation–SFT interaction in Cu (4, 12, 20), the obstacles can be absorbed or partially absorbed at high temperature but not at low temperature. In tensile experiments on steels, the dominant deformation mechanism is found to change from twinning to dislocation channeling with increasing temperature (21, 22). In tensile experiments on Zircaloy-2, the width of the dislocation channels is observed to be larger at high temperature than at low temperature (26). These various deformation mechanisms shown in Fig. 7 now can be viewed as an underlying competition of strain rate and thermal activation in the spirit of the mechanism map in Fig. 6. We anticipate a similar theoretical framework can be developed to quantitatively predict the boundaries separating interaction mechanisms in any material or defect system as those exemplified in Fig. 7. Although the original ABC algorithm (34) has been used here, significant improvements to the efficiency of the method (43) can enable the investigation of more complex microstructures such as grain boundaries and cracks. Comparing Figs. 6 and 7, we see a unifying role for the mechanism map to guide future simulation and experimental investigations.

A final observation is that we have demonstrated the feasibility of simulating plastic deformation involving elementary dislocation–defect interactions at the atomic scale at low strain rates. This contribution bridges the gap between atomistic simulations and mesoscale models of plasticity in enabling the prediction of deformation mechanisms and kinetics over a very wide range of strain rates and time scales (44). There is considerable potential for future work in extending the present approach to other crystalline defects, such as cracks and grain boundaries (replacing the dislocation) as part of the current attempts to study technologically significant macroscale phenomena using atomic-level mechanisms (45). In particular we see the coupling of strain rate and thermal activation as a fundamental physical principle that governs nonequilibrium reaction mechanisms driven by time-dependent conditions, applicable not only to defect interactions but also broadly to other fields ranging from rheology (46) to electrochemistry (47).

Methods

Combining ABC and TST in Simulating Dislocation–Obstacle Interactions at Prescribed Strain Rate and Temperature. The algorithm that we constructed to simulate the dislocation–defect interactions at any given strain rate and temperature follows the steps described below. The imposed constant strain rate in simulations mimics tensile test experiments performed under constant strain rate conditions:

i) under a given strain condition (including the initial state with no strain), use ABC to obtain the reaction pathway;

ii) apply nudged elastic band method (48) to calculate the energy barrier E_b between the initial and final states that are determined in step *i*; and

iii) determine the thermal activation time defined as $\Delta t = \left[\nu_0 e^{-E_b/k_B T}\right]^{-1}$, where ν_0 is the attempt frequency (of order 10^{13} s^{-1}). For a specified strain rate $\dot{\varepsilon}$, the corresponding strain increment, $\Delta\varepsilon = \dot{\varepsilon}\Delta t = \dot{\varepsilon}\left[\nu_0 e^{-E_b/k_B T}\right]^{-1}$, is applied to the system. Go back to step *i* under the new strain condition.

In this algorithm the coupling between thermal activation and strain rate is treated in the TST framework. Notice the system is strained in discrete steps of variable magnitude at time increments. Because strain loading is continuous in actual experiments, appreciable errors could arise if the calculated strain increment, $\Delta\varepsilon$, in step *iii* is too large. The errors come from two aspects: (a) the system can be driven too far from current state, and some abrupt changes to the inherent structures and underlying potential energy landscape might happen, and (b) the activation barrier can vary as a function of time/strain; therefore, the calculated strain increment based on identified barrier under a fixed time/strain can induce errors on timescale estimations. The timescale can be overestimated or underestimated, depending on whether

the activation barrier decreases or increases with time/strain. To control the errors, a cutoff value on maximum strain allowed is imposed. For the problem at hand, ε_s is determined by considering the error in the convergence of the critical resolved shear stress and the atomic configurations during and after the interaction (49). To optimize computational efficiency and accuracy, the value of ε_s is set at 5×10^{-4} in this study, which gives an error of less than 5% of the critical stress. If the calculated $\Delta\varepsilon$ is smaller than ε_s, then the transition is accepted and the incremental strain $\Delta\varepsilon$ is applied. If the calculated strain increment is larger than ε_s, then only an incremental strain of ε_s ($\Delta\varepsilon = \varepsilon_s$) is induced into the system, whereas the transition event is not accepted by putting the system into the same configuration and the calculation continues at step *i*.

System Setup and Details of the ABC and MD Simulations. The modeled system in Zr contains an $1/3<11\bar{2}0>\{1\bar{1}00\}$ edge dislocation and a 5-SIA cluster in the basal plane. This system is equivalent to the one studied earlier by static simulation (1). The simulation crystal has the dimensions of 14.46 nm, 4.15 nm, and 13.51 nm along the dislocation Burgers vector, along the dislocation line, and perpendicular to the dislocation slip plane, respectively, and contains 34,181 mobile Zr atoms. The periodic boundary conditions are applied along the dislocation line and Burgers vector directions, whereas atoms in the upper and lower blocks were fixed (Fig. 1). The upper block was moved as a whole with a certain velocity providing the required strain rate. Under each strain rate, the x-component of the total force F_x on the upper block is calculated. Then the stress is calculated as F_x/S_{xy}, where S_{xy} is top surface area of the upper block. More details of the model, strain application, and applied stress calculations can be found in ref. 4 and references there. Exactly the same crystals were used for ABC and MD simulations. An embedded atom method–type interatomic potential for hcp Zr metal, the AWB95 potential (50), is used in this study.

The classical MD simulations are performed under three different strain rates ($10^5\ s^{-1}$, $10^6\ s^{-1}$, $10^7\ s^{-1}$), and eight different temperatures (50 K, 150 K, 200 K, 250 K, 300 K, 350 K, 400 K, and 500 K) at each strain rate. We have used the NVE ensemble while adjusting the lattice parameter to zero total pressure at each temperature. The performed set of MD simulations is very expensive computationally; for the low strain rate cases up to $\sim3\times10^7$ steps are needed in integrating the Newton's equation of motion to cover physical times of up to ~150 ns.

ACKNOWLEDGMENTS. This work was supported by the Consortium for Advanced Simulation of Light Water Reactors, an Energy Innovation Hub for Modeling and Simulation of Nuclear Reactors under US Department of Energy Contract DE-AC05-00OR22725, and Y.N.O. was supported by the Division of Materials Sciences and Engineering, US Department of Energy.

1. Voskoboynikov RE, Osetsky YN, Bacon DJ (2005) Self-interstitial atom clusters as obstacles to glide of edge dislocations in α-zirconium. *Mater Sci Eng A* 400–401(0):54–58.
2. Griffiths M (1993) Evolution of microstructure in hcp metals during irradiation. *J Nucl Mater* 205(0):225–241.
3. Hayes T, Kassner M (2006) Creep of zirconium and zirconium alloys. *Metallurgical and Materials Transactions A* 37(8):2389–2396.
4. Bacon DJ, Osetsky YN, Rodney D (2009) Dislocation–obstacle interactions at the atomic level. *Dislocations in Solids*, eds Hirth JP, Kubin L (Elsevier, Amsterdam), Vol 15, Chap 88, pp 1–90.
5. Frost HJ, Ashby MF (1982) *Deformation-Mechanism Maps: The Plasticity and Creep of Metals and Ceramics* (Pergamon, Oxford).
6. Zhu T, Li J (2010) Ultra-strength materials. *Prog Mater Sci* 55(7):710–757.
7. Yamakov V, Wolf D, Phillpot SR, Mukherjee AK, Gleiter H (2004) Deformation-mechanism map for nanocrystalline metals by molecular-dynamics simulation. *Nat Mater* 3(1):43–47.
8. Onimus F, Monnet I, Béchade JL, Prioul C, Pilvin P (2004) A statistical TEM investigation of dislocation channeling mechanism in neutron irradiated zirconium alloys. *J Nucl Mater* 328(2-3):165–179.
9. Onimus F, Béchade J-L (2009) A polycrystalline modeling of the mechanical behavior of neutron irradiated zirconium alloys. *J Nucl Mater* 384(2):163–174.
10. Dunlop JW, Bréchet YJM, Legras L, Estrin Y (2007) Dislocation density-based modelling of plastic deformation of Zircaloy-4. *Mater Sci Eng A* 443(1-2):77–86.
11. Terentyev D, Osetsky YN, Bacon DJ (2010) Competing processes in reactions between an edge dislocation and dislocation loops in a body-centred cubic metal. *Scr Mater* 62(9):697–700.
12. Bacon DJ, Osetsky YN, Rong Z (2006) Computer simulation of reactions between an edge dislocation and glissile self-interstitial clusters in iron. *Philos Mag* 86(25-26): 3921–3936.
13. Hatano T, Matsui H (2005) Molecular dynamics investigation of dislocation pinning by a nanovoid in copper. *Phys Rev B* 72(9):094105.
14. Monnet G (2007) Mechanical and energetical analysis of molecular dynamics simulations of dislocation–defect interactions. *Acta Mater* 55(15):5081–5088.
15. Kioussis NG, Ghoniem NM (2010) Modeling of dislocation interaction with solutes, nano-precipitates and interfaces: A multiscale challenge. *Journal of Computational and Theoretical Nanoscience* 7(8):1317–1346.
16. Weinberger CR, Jennings AT, Kang K, Greer JR (2012) Atomistic simulations and continuum modeling of dislocation nucleation and strength in gold nanowires. *J Mech Phys Solids* 60(1):84–103.
17. Zhu T, Li J, Samanta A, Leach A, Gall K (2008) Temperature and strain-rate dependence of surface dislocation nucleation. *Phys Rev Lett* 100(2):025502.
18. Fan Y, Osetsky YN, Yip S, Yildiz B (2012) Onset mechanism of strain-rate-induced flow stress upturn. *Phys Rev Lett* 109(13):135503.
19. Monnet G, Osetsky YN, Bacon DJ (2010) Mesoscale thermodynamic analysis of atomic-scale dislocation–obstacle interactions simulated by molecular dynamics. *Philos Mag* 90(7-8):1001–1018.
20. Osetsky YN, Rodney D, Bacon DJ (2006) Atomic-scale study of dislocation–stacking fault tetrahedron interactions. Part I: Mechanisms. *Philos Mag* 86(16):2295–2313.
21. Bruemmer SM, Cole JI, Carter RD, Was GS (1996) Defect microstructures and deformation mechanisms in irradiated austenitic stainless steels. *MRS Proceedings Library* 439(b):437.
22. Hashimoto N, Zinkle SJ, Rowcliffe AF, Robertson JP, Jitsukawa S (2000) Deformation mechanisms in 316 stainless steel irradiated at 60°C and 330°C. *Journal of Nuclear Materials* 283–287(Part 1):528–534.
23. Matsukawa Y, Zinkle SJ (2004) Dynamic observation of the collapse process of a stacking fault tetrahedron by moving dislocations. *Journal of Nuclear Materials* 329–333(Part B):919–923.
24. Robach JS, Robertson IM, Wirth BD, Arsenlis A (2003) In-situ transmission electron microscopy observations and molecular dynamics simulations of dislocation-defect interactions in ion-irradiated copper. *Philos Mag* 83(8):955–967.
25. Osetsky YN, Matsukawa Y, Stoller RE, Zinkle SJ (2006) On the features of dislocation–obstacle interaction in thin films: Large-scale atomistic simulation. *Philos Mag Lett* 86(8):511–519.
26. Onchi T, Kayano H, Higashiguchi Y (1980) The inhomogeneous deformation behaviour of neutron irradiated Zircaloy-2. *J Nucl Mater* 88(2-3):226–235.
27. Cole JI, Bruemmer SM (1995) Post-irradiation deformation characteristics of heavy-ion irradiated 304L SS. *J Nucl Mater* 225(0):53–58.
28. Mousseau N, et al. (2012) The activation-relaxation technique: ART nouveau and kinetic ART. *J At Mol Opt Phys* 2012:925278.
29. Xu H, Osetsky YN, Stoller RE (2011) Simulating complex atomistic processes: On-the-fly kinetic Monte Carlo scheme with selective active volumes. *Phys Rev B* 84(13):132103.
30. Voter AF (1997) A method for accelerating the molecular dynamics simulation of infrequent events. *J Chem Phys* 106(11):4665–4677.
31. Laio A, Parrinello M (2002) Escaping free-energy minima. *Proc Natl Acad Sci USA* 99(20):12562–12566.
32. Ishii A, Ogata S, Kimizuka H, Li J (2012) Adaptive-boost molecular dynamics simulation of carbon diffusion in iron. *Phys Rev B* 85(6):064303.
33. Wang H, Xu DS, Rodney D, Veyssière P, Yang R (2013) Atomistic investigation of the annihilation of non-screw dislocation dipoles in Al, Cu, Ni and γ -TiAl. *Model Simul Mater Sci Eng* 21(2):025002.
34. Kushima A, et al. (2009) Computing the viscosity of supercooled liquids. *J Chem Phys* 130(22):224504–224512.
35. Fan Y, Kushima A, Yildiz B (2010) Unfaulting mechanism of trapped self-interstitial atom clusters in bcc Fe: A kinetic study based on the potential energy landscape. *Phys Rev B* 81(10):104102.
36. Lau TT, Kushima A, Yip S (2010) Atomistic simulation of creep in a nanocrystal. *Phys Rev Lett* 104(17):175501.
37. Fan Y, Kushima A, Yip S, Yildiz B (2011) Mechanism of void nucleation and growth in bcc Fe: Atomistic simulations at experimental time scales. *Phys Rev Lett* 106(12):125501.
38. Li J, et al. (2011) Computing the viscosity of supercooled liquids: Markov network model. *PLoS ONE* 6(3):e17909.
39. Wooding SJ, Howe LM, Gao F, Calder AF, Bacon DJ (1998) A molecular dynamics study of high-energy displacement cascades in α-zirconium. *J Nucl Mater* 254(2-3):191–204.
40. Edwards DJ, Singh BN, Bilde-Sørensen JB (2005) Initiation and propagation of cleared channels in neutron-irradiated pure copper and a precipitation hardened CuCrZr alloy. *J Nucl Mater* 342(1-3):164–178.
41. Khater HA, Bacon DJ (2010) Dislocation core structure and dynamics in two atomic models of α-zirconium. *Acta Mater* 58(8):2978–2987.
42. Wirth BD, Bulatov VV, De La Diaz Rubia T (2002) Dislocation-stacking fault tetrahedron interactions in Cu. *J Eng Mat Technol* 124(3):329–334.
43. Cao P, Li M, Heugle RJ, Park HS, Lin X (2012) Self-learning metabasin escape algorithm for supercooled liquids. *Phys Rev E Stat Nonlin Soft Matter Phys* 86(1 Pt 2):016710.
44. Crabtree GW, Sarrao JL (2012) Opportunities for mesoscale science. *MRS Bull* 37(11): 1079–1088.
45. Song J, Curtin WA (2013) Atomic mechanism and prediction of hydrogen embrittlement in iron. *Nat Mater* 12(2):145–151.
46. Rottler J, Robbins MO (2003) Shear yielding of amorphous glassy solids: Effect of temperature and strain rate. *Phys Rev E* 68(1):011507.
47. Bazant MZ (2013) Theory of chemical kinetics and charge transfer based on nonequilibrium thermodynamics. *Acc Chem Res* 46(5):1144–1160.
48. Henkelman G, Jonsson H (2000) Improved tangent estimate in the nudged elastic band method for finding minimum energy paths and saddle points. *J Chem Phys* 113(22):9978–9985.
49. Osetsky YN, Bacon DJ (2003) An atomic-level model for studying the dynamics of edge dislocations in metals. *Model Simul Mater Sci Eng* 11(4):427.
50. Ackland GJ, Wooding SJ, Bacon DJ (1995) Defect, surface and displacement-threshold properties of α-zirconium simulated with a many-body potential. *Philos Mag A* 71(3): 553–565.